Examining the Relationship between Tropopause Polar Vortices and Tornado Outbreaks

Matthew T. Bray, a Steven M. Cavallo, and Howard B. Bluestein

^a School of Meteorology, University of Oklahoma, Norman, Oklahoma

(Manuscript received 8 April 2021, in final form 22 July 2021)

ABSTRACT: Midlatitude jet streaks are known to produce conditions broadly supportive of tornado outbreaks, including forcing for large-scale ascent, increased wind shear, and decreased static stability. Although many processes may initiate a jet streak, we focus here on the development of jet maxima by interactions between the polar jet and tropopause polar vortices (TPVs). Originating from the Arctic, TPVs are long-lived circulations on the tropopause, which can be advected into the midlatitudes. We hypothesize that when these vortices interact with the jet, they may contribute supplemental forcing for ascent and shear to tornado outbreaks, assuming other environmental conditions supportive of tornado development exist. Using a case set of significant tornado outbreak days from three states—Oklahoma, Illinois, and Alabama—we show that a vortex—jet streak structure is present (within 1250 km) in around two-thirds of tornado outbreaks. These vortices are commonly Arctic in origin (i.e., are TPVs) and are advected through a consistent path of entry into the midlatitudes in the week before the outbreak, moving across the northern Pacific and into the Gulf of Alaska before turning equatorward along the North American coast. These vortices are shown to be more intense and longer-lived than average. We further demonstrate that statistically significant patterns of wind shear, quasigeostrophic forcing for ascent, and low static stability are present over the outbreak regions on the synoptic scale. In addition, we find that TPVs associated with tornadic events occur most often in the spring and are associated with greater low-level moisture when compared to nontornadic TPV cases.

SIGNIFICANCE STATEMENT: Tornado outbreaks over the United States have the potential to cause significant loss of life and property. To ensure adequate preparation time and minimize these losses, forecasting these events well before their occurrence is essential; however, it is currently difficult to predict tornado outbreaks more than a few days in advance. This work investigates a potential connection between atmospheric features known as tropopause polar vortices (TPVs) and tornado outbreaks in the United States. Due to their physical characteristics, TPVs have the potential to be forecasted up to weeks in advance. Although further work will be needed to confirm this link, our findings could provide a tool for long-term prediction of future tornado outbreaks.

KEYWORDS: Arctic; Severe storms; Synoptic-scale processes; Potential vorticity; Tropopause; Operational forecasting

1. Introduction

Environments favorable for the development of severe thunderstorms are traditionally expected to possess four key elements: adequate low-level moisture, sufficient vertical wind shear, low static stability, and some type of lifting mechanism (Weisman and Klemp 1982; Johns and Doswell 1992; Doswell et al. 1996). These conditions may derive from forcings on a range of spatial and temporal scales, but for the present study, we focus mainly on synoptic-scale influences. Previous work has shown that in the United States, certain synoptic patterns, particularly those with a trough to the west, a strong jet aloft, and a surface cyclone, are most conducive to tornado outbreaks (Mercer et al. 2012). These conditions bolster tornado probabilities by introducing reduced static stability, stronger vertical wind shear, and increased upward motion (Doswell et al. 1993). In addition, several studies have demonstrated that external factors acting on longer time scales, like the Madden-Julian oscillation, El Niño-Southern Oscillation, and variations in atmospheric angular momentum, can alter the synoptic structure of the atmosphere and indirectly produce discernible

Corresponding author: Matthew T. Bray, matthewbray1@ou.edu

changes in severe weather patterns (Thompson and Roundy 2013; Barrett and Gensini 2013; Cook et al. 2017; Gensini and Marinaro 2016; Gensini et al. 2019; Miller et al. 2020; Moore and McGuire 2020; Gensini et al. 2020).

Due to their association with middle-troposphere vertical velocity generation and enhanced wind shear, jet streaks have been widely studied as important factors in tornado outbreaks (Uccellini and Johnson 1979; Bluestein and Thomas 1984; Sanders and Blanchard 1993). Moreover, previous studies have shown that jet streak generation is often closely linked to enhanced potential vorticity (PV) gradients generated by tropopause PV anomalies that interact with the jet (Bosart et al. 1996; Hakim 2000; Pyle et al. 2004). In this study, we aim to extend this previous knowledge to a particular subset of PV anomalies: tropopause polar vortices (TPVs) (Hakim and Canavan 2005; Cavallo and Hakim 2010). Although TPVs are Arctic in origin, they can be advected to the midlatitudes, where they may assist in the development of jet streaks and thus serve as a catalyst for tornado-producing storms (Pyle et al. 2004).

Jet streaks have been extensively studied and used in an operational capacity to assist in the forecasting of tornado outbreaks. A theoretical model for this connection was first presented by Beebe and Bates (1955), who demonstrated the relationship

between jet streaks aloft and background environments amenable to the development of convection, via the creation of deep vertical shear and forcing for ascent. This pattern also emerged during several observed cases (Uccellini and Johnson 1979; Bluestein and Thomas 1984; Sanders and Blanchard 1993), in which various jetrelated factors were noted to initiate and bolster convection. These studies revealed other jet streak related antecedents for storm initiation, including decreased static stability by differential advection of cold air aloft (Uccellini and Johnson 1979), enhanced vertical wind shear, and intensified moisture convergence near the surface (Bluestein and Thomas 1984). Later modeling-based studies further demonstrated the dependence of these conditions on the curvature of the jet, which may substantially alter the location of vertical motion and low static stability relative to the jet streak (Moore and VanKnowe 1992). More recent climatological studies comparing tornado locations to jet streaks revealed favored locations for tornado development relative to the jet maximum, namely, in the left, and less frequently right, exit regions (Rose et al. 2004; Clark et al. 2009).

Of particular interest in the present study is the generation of jet streaks via interactions between a jet and PV anomalies on the tropopause. This process, driven by enhanced baroclinicity and strong PV gradients in the region of juxtaposition, has been observed in numerous case studies of high-impact weather events (Bosart et al. 1996; Hakim et al. 1995, 1996). Hakim (2000) further demonstrated that the PV anomalies possess a vortex-like structure and showed a direct relation between anomaly intensity and jet streak velocity. Pyle et al. (2004) validated this relationship, providing multiple examples of jet streak intensification in the presence of tropopause anomalies. This jet strengthening was associated with a tightened potential temperature gradient and was found to be confined to periods of close proximity between the jet streak and PV anomaly (Pyle et al. 2004). While it has been established that PV anomalies may induce jet streaks through interactions with a jet stream, and therefore play a role in high-impact weather events, the origin and development of these anomalies has never been explicitly studied.

The development of jet maxima driven by PV anomalies may also be viewed through the lens of jet superpositions. Vertical superpositions between the subtropical and polar jets have been described in detail by Winters and Martin (2017), and are known to be associated with significant weather events (Winters and Martin 2016). Winters and Martin (2017) also found that this subtropical-polar superposition process generally requires a polar cyclonic PV anomaly that is displaced to the midlatitudes, a role which may be fulfilled by a TPV or similar vortex. It is also possible, though, that TPVs may initiate a jet superposition event upon interaction with the polar jet without subtropical influence. The circulation about TPVs may be termed as the Arctic jet (e.g., Shapiro et al. 1987), and thus jet maxima can be created via a polar-Arctic jet superposition. Although the dynamical and physical properties of such a superposition event have not yet been studied, we expect that they may follow closely to the superposition model proposed by Winters and Martin (2017).

Although jet development as described above could occur with any tropospheric PV anomaly, the primary focus of this

study is on TPVs, which can be especially long-lived and thus may eventually provide an extended range severe weather forecasting tool (Cavallo and Hakim 2013). TPVs arise in the Arctic where, in the absence of strong vertical shear, vortices can persist for periods sometimes exceeding one month (Hakim and Canavan 2005). TPVs may be cold-core cyclonic or warm-core anticyclonic, though cyclonic vortices are more common and generally more significant in influencing surface weather (Hakim and Canavan 2005; Cavallo and Hakim 2009). Cyclonic TPVs are characterized by high pressure and low potential temperature on the dynamic tropopause, defined by the 2 potential vorticity unit (PVU; 1 PVU = $10^{-6} \text{K kg}^{-1} \text{m}^2 \text{s}^{-1}$) surface (Cavallo and Hakim 2009). Examining TPVs as potential vorticity anomalies on the dynamic tropopause has the advantage of conveying information about these conserved vortices with a single map. In contrast, examining such features as potential vorticity anomalies on isentropic surfaces often requires several maps at different levels to fully describe the system (Morgan and Nielson-Gammon 1998). Cavallo and Hakim (2010, 2012) have illustrated the importance of diabatic processes, especially radiative cooling, in sustaining TPVs. As with midlatitude PV anomalies, TPVs have been shown to facilitate surface cyclogenesis and function similarly to other tropospheric disturbances when interacting with a jet (Simmonds and Rudeva 2014; Cavallo and Hakim 2010). This study investigates whether TPVs are a potential source of jet-streakcreating PV anomalies.

Despite the established connection between PV anomalies, jet streaks, and tornado outbreaks, a clear examination of the PV anomalies fulfilling this role has yet to be conducted. The purpose of this study is to demonstrate a statistical relationship between TPVs (and other PV anomalies) in the midlatitudes and tornado outbreaks and to explore the characteristics of these vortices prior to their jet interactions. This will act as a first step toward showing a physical relationship, which can be expanded upon by future modeling studies. We hypothesize that these PV anomalies may be associated with jet streaks present during major tornado events, which may enhance upward vertical motion over outbreak areas. Moreover, it is expected that differential vertical temperature advection by the jet streak will result in decreased static stability. Similarly, additional flow aloft increases vertical shear and, in conjunction with associated surface features, promotes high environmental storm relative helicity. It is important to note, however, that TPVs and similar PV anomalies are not expected to be sufficient to produce tornado outbreaks. Instead, they are hypothesized to provide supplementary forcing for ascent, shear, and instability in environments that possess other severe storm precursors.

A simplified conceptual model of this mechanism in the case of a straight, polar-Arctic jet superposition is provided in Fig. 1. As a cyclonic PV anomaly enters the midlatitudes and is advected equatorward, it interacts with a westerly jet. The westerly portion of the TPV circulation on the equatorward side of the vortex eventually becomes superimposed with the jet (this could also be viewed as the TPV amplifying the existing PV gradient associated with the jet), creating a jet streak. Drawing from the classic four-quadrant straight jet streak model

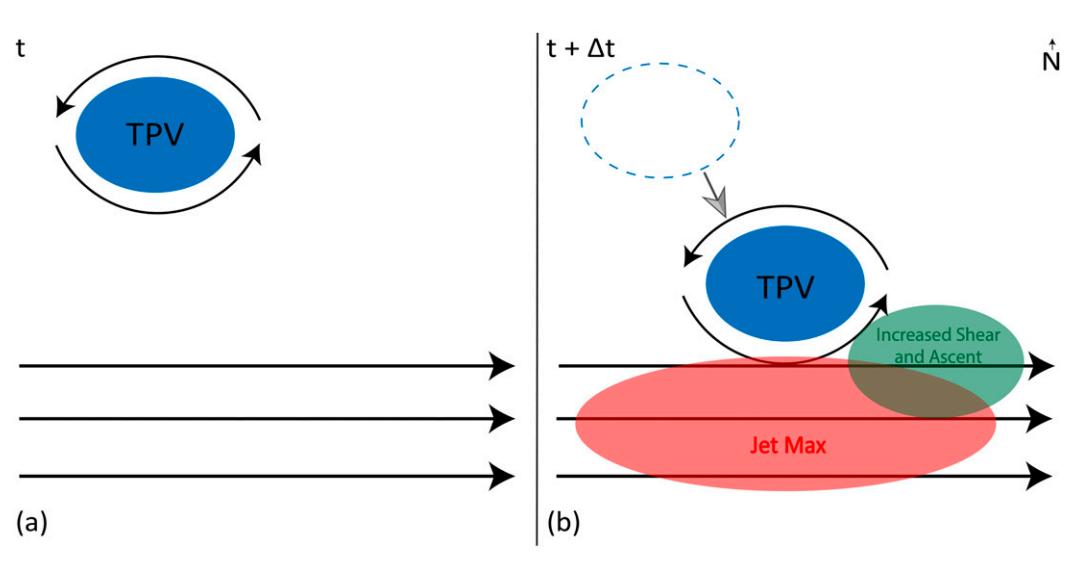


FIG. 1. A conceptual model of the proposed TPV-jet mechanism for generating jet streaks and favorable conditions for tornadoes, for a straight polar jet case. (a) A TPV enters the midlatitudes via advection (represented by the heavy gray arrow) and approaches an existing jet. (b) A portion of the circulation around the TPV becomes superimposed on the existing jet, creating a jet streak. Based on the classic four-quadrant jet streak model, this creates regions of enhanced shear and large-scale ascent.

(Uccellini and Kocin 1987), such a feature will produce a broad region of increased wind shear along with forcing for ascent in the left exit and right entrance regions (though the former will prove to be more often associated with the outbreaks in this study). It is important to note, however, that the majority of real-world cases feature curved jets, which complicate the dynamical situation substantially. Moreover, in most real-world cases, the TPV will interact with an already perturbed jet. In such cases, the TPV may help to initiate or be affected by Rossby wave break events. Still, this simple model provides a rough outline of the hypothesized processes. When combined with other features such as surface moisture convergence and surface lifting mechanisms, we predict that these jet-related synoptic-scale features contribute to favorable conditions for thunderstorm and tornado development. In addition, we expect that vortices entering the United States will exhibit a preferred entry pathway or common vortex characteristics, which would be helpful for forecasting applications.

The remainder of this paper is organized as follows. Section 2 outlines the methodology of the study, including case identification, TPV tracking, quasigeostrophic analysis techniques, and null case examination. Section 3 provides results for the selected tornado outbreak cases, as well as an examination of null cases. Section 4 includes a summary, conclusions from the study, and recommendations for future work.

2. Methods

a. Case identification

Tornado reports from 1979 to 2019 across the continental United States taken from the Storm Prediction Center are used as an indicator of tornado frequency. It is important to note that this database has well-established limitations. Damage

estimates can vary based on the assessor, while an increasingly dense spotter network has led to a relative uptick in tornado reports in recent years (Verbout et al. 2006). For the purposes of the present study, though, this dataset provides an acceptable metric for classifying tornado event days. Clusters of tornado activity are defined as local maxima in an empirical probability distribution of tornado occurrences generated from these data (Fig. 2). This clustering procedure allows for geographic compositing of outbreak events and for easy investigation of the dynamics at play in outbreaks in different regions. To isolate dominant clusters within the distribution, only maxima with a probability density exceeding two standard deviations from the mean are considered. Using the two standard deviation

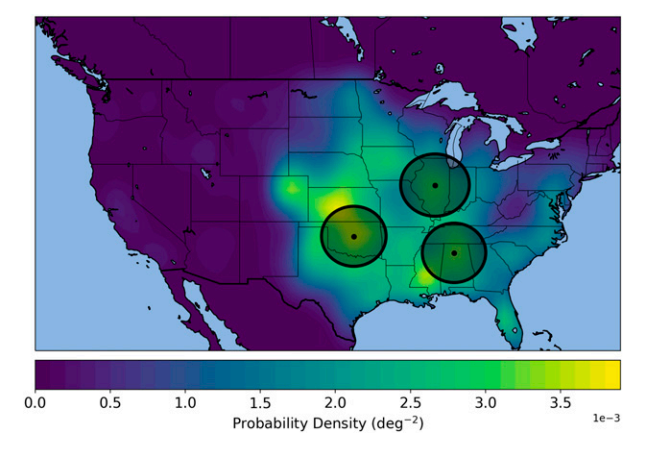


FIG. 2. A probability density map of all tornadoes in the United States from 1979 to 2019 calculated using a Gaussian kernel density estimator. The regions of radius 300 km defining each cluster used in the analysis are shown in black.

probability maxima criterion, a total of five clusters across the United States are created. To avoid overlapping outbreak events between each cluster, an event radius of 300 km is established around each probability maximum to create a cluster region. The 300-km threshold was chosen based on sensitivity tests; smaller radii tended to exclude pertinent events, while larger radii often grouped notably distant (and thus difficult to composite accurately) events into one cluster.

Following work by Cook and Schaefer (2008) and Thompson and Roundy (2013), we define a significant tornado outbreak day as a 24-h period (1200–1200 UTC) in which 6 or more tornadoes of at least F2/EF2 (depending on the year of the report) intensity are reported within a given cluster region. This definition is particularly useful for this study, as it disregards relatively weak tornadoes and small outbreaks, which are less likely to be tied to the synoptic-scale features we examine here, and favors highimpact events (Thompson and Roundy 2013). Any tornado track which starts or ends within the specified cluster region is counted toward the outbreak totals. Although the tornado track data extends back to 1950, we choose to limit our study to outbreaks from 1979 to 2019 both to align with the availability of ERA-Interim data (to be discussed in more detail in the next section) and because tornado verification data are substantially more reliable during this period (Tippett et al. 2015).

b. TPV tracking

For each case, local maxima in the tropopause-level wind speed are determined using ERA-Interim data (Dee et al. 2011). The nearest of these local wind speed maxima to the outbreak location that is also west of any part of the outbreak region is taken as the jet streak associated with the case. The tropopause PV anomaly closest to this jet streak, determined using a repository of all such anomalies in the Northern Hemisphere from Szapiro and Cavallo (2018), is selected as the PV anomaly associated with the case. To account for pathways into the midlatitudes and analyze the impact of TPVs on midlatitude weather, a relaxed version of the definition of a TPV from Hakim and Canavan (2005) is used; for the purposes of this study, PV anomalies which form north of 60°N will be considered TPVs, while other vortices will be broadly called PV anomalies. This track repository contains information on TPV and PV anomaly locations and intensities; however, it does not take into account vortex mergers and splits. In lieu of this, a tracking algorithm developed for this study includes methods to analyze splitting events and merge the tracks of pre- and post-split TPVs.

Vortex splits within the track file are identified within a potential split area around the last known vortex location, approximating the maximum distance the anomaly could have covered during the 6-h time step between the records in the file. If a new PV anomaly is found within this radius at the previous time step (i.e., 6 h before the vortex under consideration), then it is possible (though not guaranteed) that a vortex split occurred during this period. An illustrative example of this process is provided in Fig. 3. The radius potential split area (the black circle in Fig. 3) is calculated using the approximate velocity of the anomaly, the Rossby deformation radius of the post-split anomaly, and the vortex radii of the pre- and

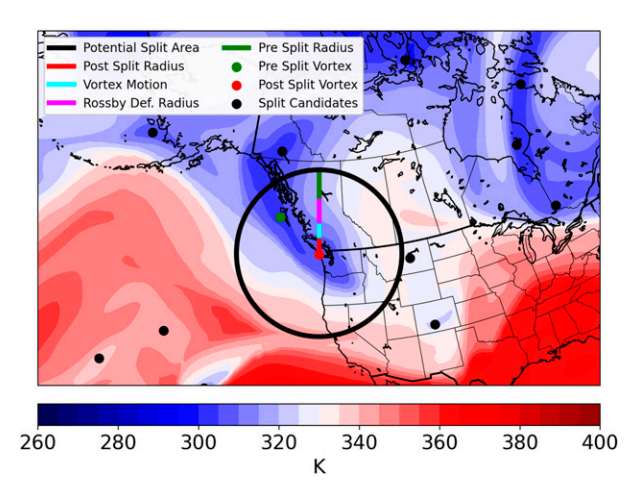


FIG. 3. An example of the vortex splitting algorithm described in the text, using a split that occurred between 1200 and 1800 UTC 2 Oct 1998 (the same TPV associated with the case study in section 3a). The background color fill shows tropopause potential temperature (K) at 1200 UTC 2 Oct 1998 (i.e., just prior to the split). The red dot shows the post-split vortex, around which the split search occurs, while the green dot identifies the pre-split vortex identified by the algorithm. Black dots show other vortices present at the time which were not near enough to the post-split vortex to be considered as the pre-split vortex. The black circle shows the potential split area around the post-split vortex. The colored segments show the contributions to this search radius from the four factors described in the text: the pre-split vortex radius (green), the post-split vortex radius (red), the Rossby deformation radius (magenta), and vortex motion (cyan).

post-split anomalies (the colored line segments in Fig. 3). This combination of parameters accounts for vortex motion, spreading, and stretching during the 6-h split window. The closest candidate out of all anomalies that fall within the potential split radius at the previous time step is taken as the pre-split vortex (the green point in Fig. 3). If a new vortex is identified, this process is repeated to construct a full vortex track, inclusive of splitting events, until no new vortex can be identified within the potential split radius. This point, sufficiently distant from other PV anomalies, is considered to be the genesis location of the vortex. Although this is not a fully comprehensive method of characterizing splits, it is computationally efficient and appears sufficiently accurate for the present study, based on several test cases.

c. Diagnosis of tropopause and middle-atmosphere conditions

Tropopause fields for each case are taken from the ERA-Interim reanalysis dataset, with the 2 PVU level specified as the dynamic tropopause (Dee et al. 2011). Synoptic monthly means data from the same reanalysis is used to establish a 30-yr climatology (1981–2010) of tropopause conditions. Composite anomalies of tropopause conditions are calculated for each cluster with these data. To quantify the contribution of the jet streak to the tornado environment on the synoptic scale, we calculate composite anomalies of vertical motion forcing, static stability, and wind shear for each cluster. One sample,

one-tailed *t* tests are used to establish statistical significance for each composite anomaly field (Wilks 2011). Moreover, we leverage the false discovery rate approach to assess field significance (Wilks 2016). Again employing ERA-Interim, we draw geopotential, temperature, and wind data from various pressure levels. To assess the synoptic forcing for vertical motion, we use the Trenberth formulation of the QG omega equation (Bluestein 1992):

$$\left(\nabla_{p}^{2} + \frac{f_{0}}{\sigma} \frac{\partial^{2}}{\partial p^{2}}\right) \omega = \frac{f_{0}}{\sigma} \left[2\left(\frac{\partial \mathbf{V}_{g}}{\partial p} \cdot \nabla_{p} \zeta_{g}\right) + \frac{\partial \mathbf{V}_{g}}{\partial p} \cdot \nabla_{p} f - 2D^{2} \frac{\partial \theta_{D}}{\partial p} \right], \tag{1}$$

where p is pressure, f_0 is the Coriolis parameter at 45°N latitude, σ is the static stability parameter (assumed to be a constant value of $2 \times 10^{-6} \,\mathrm{m}^2 \,\mathrm{Pa}^{-2} \,\mathrm{s}^{-2}$), \mathbf{V}_g is the geostrophic wind, ζ_g is geostrophic relative vertical vorticity, D is the magnitude of deformation in the flow, and θ_D is the angle between the axis of dilatation and the x axis. We utilize the Trenberth form in this case as our analysis is focused primarily on ascent generated vorticity advection rather than by temperature advection. Compared to other forms of the QG omega equation, the Trenberth form allows for a more detailed exploration of this vorticity-driven component. We calculate the synoptic forcing for ascent at the 700-hPa level, using data from the 500-, 700-, and 900-hPa levels. Gaussian smoothing is applied to the resulting field to reduce the noise produced by inertia-gravity waves present in the result. By the sign convention of the calculation, positive values of the forcing function on the right-hand side of (1), which will be plotted below, correspond to forcing for ascent. Synoptic-scale bulk wind shear is evaluated as the magnitude of the vector difference in the 500- and 900-hPa winds. The environmental static stability is assessed using the static stability parameter at the 700-hPa level. Because we are analyzing storm (or slightly pre-storm) environments, we assume generally saturated conditions in the middle atmosphere, and so equivalent potential temperature used in place of potential temperature to incorporate moisture contributions (Bluestein 1992):

$$\sigma = -\frac{R_d T}{p} \frac{d \ln \theta_e}{dp},\tag{2}$$

where R_d is the gas constant for dry air, T is temperature at 700 hPa, p is pressure at 700 hPa, and θ_e is equivalent potential temperature.

d. Null cases

To further explore the impact of PV anomalies on tornado outbreaks, it is necessary to look at a set of null cases. Specifically, we will look at events in which a TPV passed over the continental United States but did not coincide with a tornado event. Because of computational constraints, for this portion of the analysis we employ a track file of only PV anomalies meeting the genesis-north-of-60°N TPV criterion (in contrast to the full PV anomaly file with split calculations described in section 2b) from 1979 to 2019. We perform this null case analysis on each cluster of tornado activity determined using the methods in section 2a. For each major outbreak (those

described in section 2a) within each cluster, we use the outbreak-associated PV anomaly (determined in section 2b) to help define a null case search area for that cluster. This circular search area is centered at the average outbreak PV anomaly location for each cluster. The distance between this mean PV anomaly location and each individual PV anomaly is calculated. The radius of the search area is twice the standard deviation of this set of distances. In short, we search for null case TPVs across the entire area in which PV anomalies were located in the significant tornado outbreak cases.

All TPVs that pass through the null case search area are considered; for TPVs which spend multiple time steps within the area, only the step nearest to the center of the search area is retained. ERA-Interim data are used to investigate atmospheric conditions in each of these cases. Due to the more restrictive nature of these TPV tracks (only PV anomalies which traveled from the Arctic to the continental United States without splitting are included), a more lenient tornado threshold is used for this portion of the study. Among cases of a TPV within the null case search area, if a tornado was reported in the associated cluster region (as defined in section 2a) within 24 h of the TPV passage, then the case is classified as a tornado case. Otherwise, the case is labeled and composited as a null case. To provide a more direct comparison between these cases and the major outbreak cases addressed above, temporal and spatial weights based on the major outbreak cases are applied to composites of the tornadic and null cases (e.g., a case with a TPV near the center of the search area occurring in the same season as the major outbreaks will be weighted more heavily than an off-season case with a TPV on the periphery of the search area). To create the weights, Gaussian kernel density estimation is applied to the outbreak case TPVs to produce approximate temporal and spatial probability distributions of these TPVs. Using these distributions, the product of the time and space probabilities for a given null case TPV is taken as its weight. This is intended to prevent cases that would be unlikely to produce tornadoes (such as a winter TPV in the Oklahoma region) from dominating the mean signal. As above, the statistical significance of these composites is calculated using a two-tailed t test along with a false discovery rate analysis to ensure field significance.

3. Results

a. Case determination and a case study

To simplify the geographic aspects of the analysis and ensure that no single outbreak day fell in two different clusters, three geographically representative clusters of the original five are selected: one centered in central Oklahoma, another in central Illinois, and a third in northern Alabama (Fig. 2; potential clusters in Kansas and Mississippi are omitted, as they slightly overlap with the Oklahoma and Alabama clusters). These three clusters include 21, 15, and 27 major outbreak events, respectively. These events range in intensity from exactly 6 F/EF2+ tornadoes (the minimum criterion for inclusion) to around 100 tornadoes and include tornadoes from multiple modes of convection. The average outbreak event included 24,

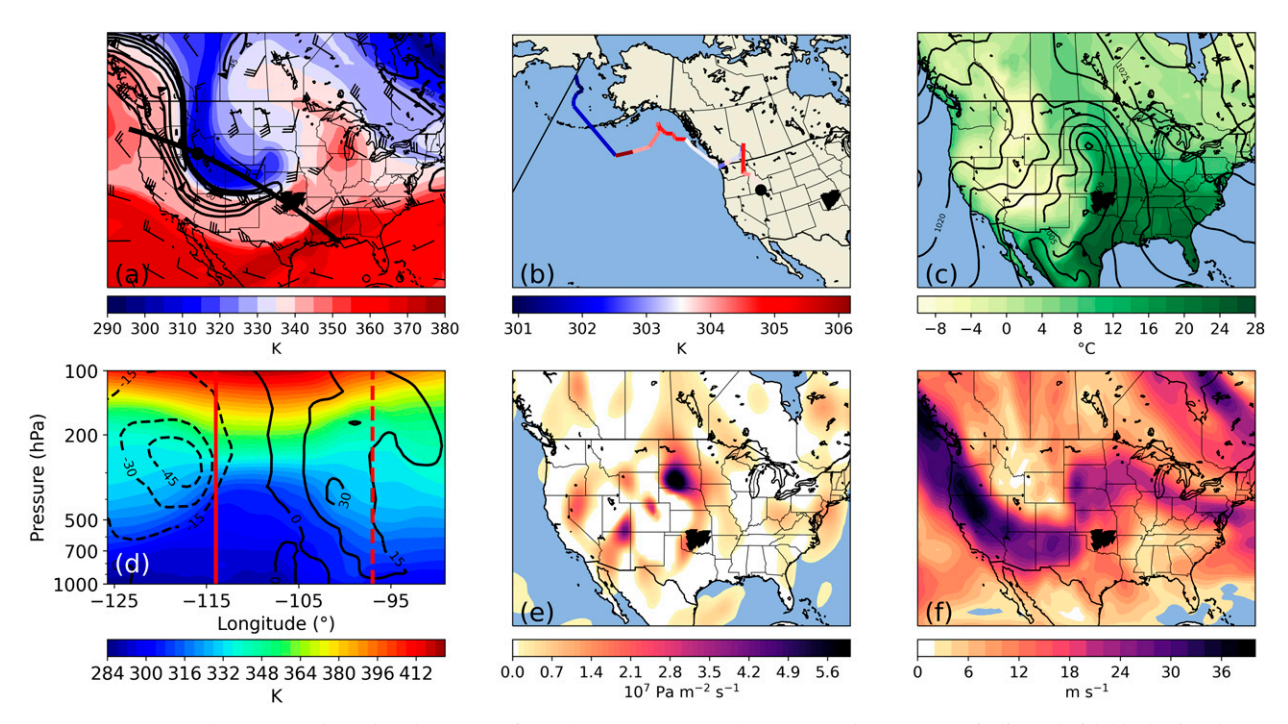


FIG. 4. A case study of a tornado outbreak at approximately 0000 UTC 4 Oct 1998. Tornado reports are indicated with black triangles on each panel. Unless otherwise noted, panels show conditions at 0000 UTC. (a) Tropopause potential temperature (fill; K), tropopause wind speeds (contour; m s⁻¹), and tropopause wind barbs. The vortex center at the time of the outbreak is indicated with a black circle over Idaho, and the path of the cross section shown in (d) is represented by a thick black line. (b) Vortex track with minimum potential temperature at 6-h intervals (line and fill; K) with the vortex location at the time of the outbreak marked by a black circle. (c) Surface dewpoint temperature (fill; C), surface mean sea level pressure (contour; hPa), and wind barbs. (d) A cross section through the tornado outbreak region (dashed red line) and TPV center (solid red line) showing potential temperature (fill; K) and cross-section normal wind speeds (contour; m s⁻¹). (e) Forcing for vertical motion at the 700-hPa level [fill; 10⁸ Pa m⁻² s⁻¹; see the methods section (section 2) for more details]. (f) Bulk wind shear magnitude in the 900–500-hPa layer (fill; m s⁻¹).

31, and 26 total tornadoes in the Oklahoma, Illinois, and Alabama clusters, respectively.

To illustrate the physical processes involved and motivate the need for a more expansive investigation, we turn to a case study of an event on 4 October 1998. In total, 26 tornadoes were reported across central Oklahoma during this event, with a total of nine strong tornadoes (EF2+). A TPV is located over southern Idaho at the time of the outbreak, approximately 0000 UTC (1900 CDT). This TPV is part of an amplified upperlevel pattern, with a Rossby wave break event potentially in progress. South of this TPV, there is a curved jet maximum, with an exit region near central Oklahoma (Fig. 4a). Though this TPV was centered over Idaho at the time of the outbreak, it can be traced back to the Bering Sea approximately 8 days earlier. The TPV moves gradually equatorward through the Gulf of Alaska, before rapidly moving into the midlatitudes just before the tornado outbreak (Fig. 4b).

While it is hypothesized that the upper-level features may enhance the severe weather environment, the essential components must also be in place near the surface. At 1900 local time (CDT) on the day of the event (Fig. 4c), a surface cyclone is present over the northern Plains, and a surface dryline is moving through western Oklahoma, providing a lifting mechanism for convection. Ample moisture is present near the

surface, and southerly flow at the surface combined with near westerly flow aloft points to a highly sheared environment (Fig. 4f). A cross section taken through the TPV and the outbreak region helps to illustrate the connection between the TPV and this shear environment, as the eastern portion of the upper-level circulation around the TPV aligns closely with the outbreak region (Fig. 4d). From a synoptic standpoint, midlevel ascent is present over most of central Oklahoma, as calculated with Eq. (1), demonstrating the alignment of lowerand upper-level features (Fig. 4e). This forcing for ascent is also notably strong over the surface cyclone, indicating that the jetinduced ageostrophic circulation may be working to strengthen the surface system, which in turn could bolster the tornado potential (Fig. 4e). Relatively low static stability is also present throughout the middle troposphere, as evidenced by vertically sloped isentropes in this layer (Fig. 4d).

The TPV associated with the event can be tracked for 8 days prior to the tornado outbreak. Vortex genesis occurs just north of 60°N, followed by a fairly rapid descent into the midlatitudes (Fig. 5a). The interactions with the jet that produce the jet streak begin around a day and a half prior to the outbreak, when the TPV is near 50°N. Throughout its lifetime, the TPV becomes gradually more anomalous as it enters the warmer midlatitude background environment, while its circulation and

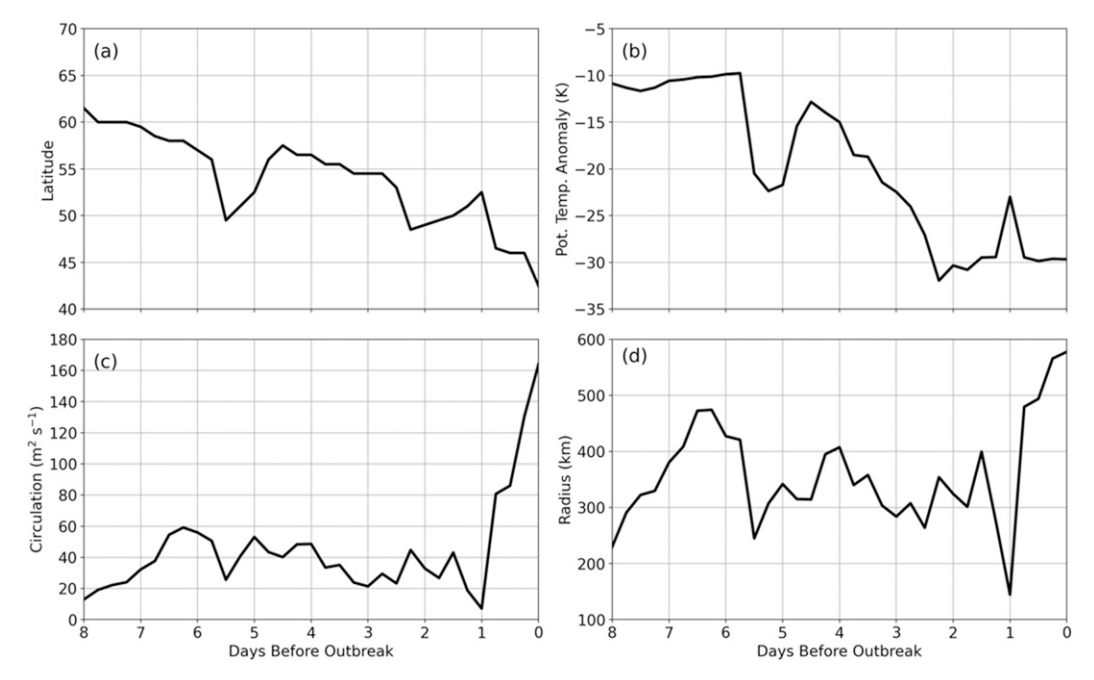


FIG. 5. (a) Vortex latitude (solid lines) for the TPV associated with the 4 Oct 1998 case study as a function of the number of days prior to the tornado outbreak. (b) As in (a), but for vortex potential temperature anomaly (K). (c) As in (a), but for vortex circulation ($m^2 s^{-1}$). (d) As in (a), but for vortex radius (km).

radius remain roughly constant until 1 day before the event, when the vortex is stretched into the midlatitudes (Fig. 5). It is also important to point out the sudden and temporary changes in potential temperature anomaly, circulation, and radius that occur exactly 1 day prior to the outbreak. These shifts are an artifact produced by the tracking algorithm in response to the deformation and splitting of the vortex during this time and do not represent true physical changes in the TPV. This case study is an example of TPV-influenced convective activity, as classic tornado ingredients combine with additional shear and ascent from the TPV-jet streak couplet to produce widespread severe weather. Further, although the curved flow makes the situation more dynamically complex (i.e., the rigid four-quadrant model of ascent and descent does not necessarily apply), this case generally aligns with the conceptual model presented in Fig. 1.

b. PV anomaly characteristics

PV anomalies are identified to the west of the outbreak location in the majority of cases studied. In a few rare cases, the identified vortex is nearly collocated with the area of convection (Fig. 6a). Of course, the presence of a PV anomaly directly above the region of interest could produce an environment high in shear and low in static stability, but these unique cases do merit a separate future study. On the whole, though, the vortices tend to be located several hundred kilometers or more away from the primary convective region, which is compatible with the jet streak model. This pattern persists across all three of the clusters studied. In the Oklahoma cases, the anomalies tend to cluster around Utah, while the Illinois vortices tend to complete their tracks over eastern Kansas and Nebraska. The anomalies in the Alabama cluster finish their tracks across a

region extending from southeastern Missouri to southern Kansas (Figs. 6b–d). Although a PV anomaly was present near the outbreak location in every case, to be called a TPV, it was stipulated in section 2b that the vortex must form north of 60°N. The nearest PV anomaly can be tracked back to this point in 13 of the 21 Oklahoma cases, 9 of the 15 Illinois cases, and 14 of the 27 Alabama cases, indicating that perhaps more than half of the PV anomalies associated with these major tornado outbreaks are Arctic in origin.

Across all three clusters, the PV anomalies exhibit the same general track into the continental United States, moving across the northern Pacific, and through the Gulf of Alaska before propagating southward (Figs. 6b-d). The Illinois cluster is somewhat anomalous, in that the vortices take a more southerly track over the Pacific (Fig. 6c). The TPVs (i.e., specifically those anomalies which begin in the Arctic) tend to form (or split from higher-latitude vortices) over north-central Russia and move eastward across Asia before following this entry pathway into the United States. The non-TPV anomalies, on the other hand, mostly form over the Northern Pacific, which is potentially indicative of Rossby wave break activity, given the high climatological frequency of Rossby wave breaks in this region (Peters and Waugh 1996; Wernli and Sprenger 2007). A limited number of TPVs across all three clusters persist for an especially long time (over 70 days in same cases), with some forming over Hudson Bay before tracking across the North Atlantic, Asia, and the Pacific. Many of these especially long-lived vortices remain stationary over the high Arctic for a portion of their lifetimes; the low shear in this region likely contributes to the long term survival of the anomalies.

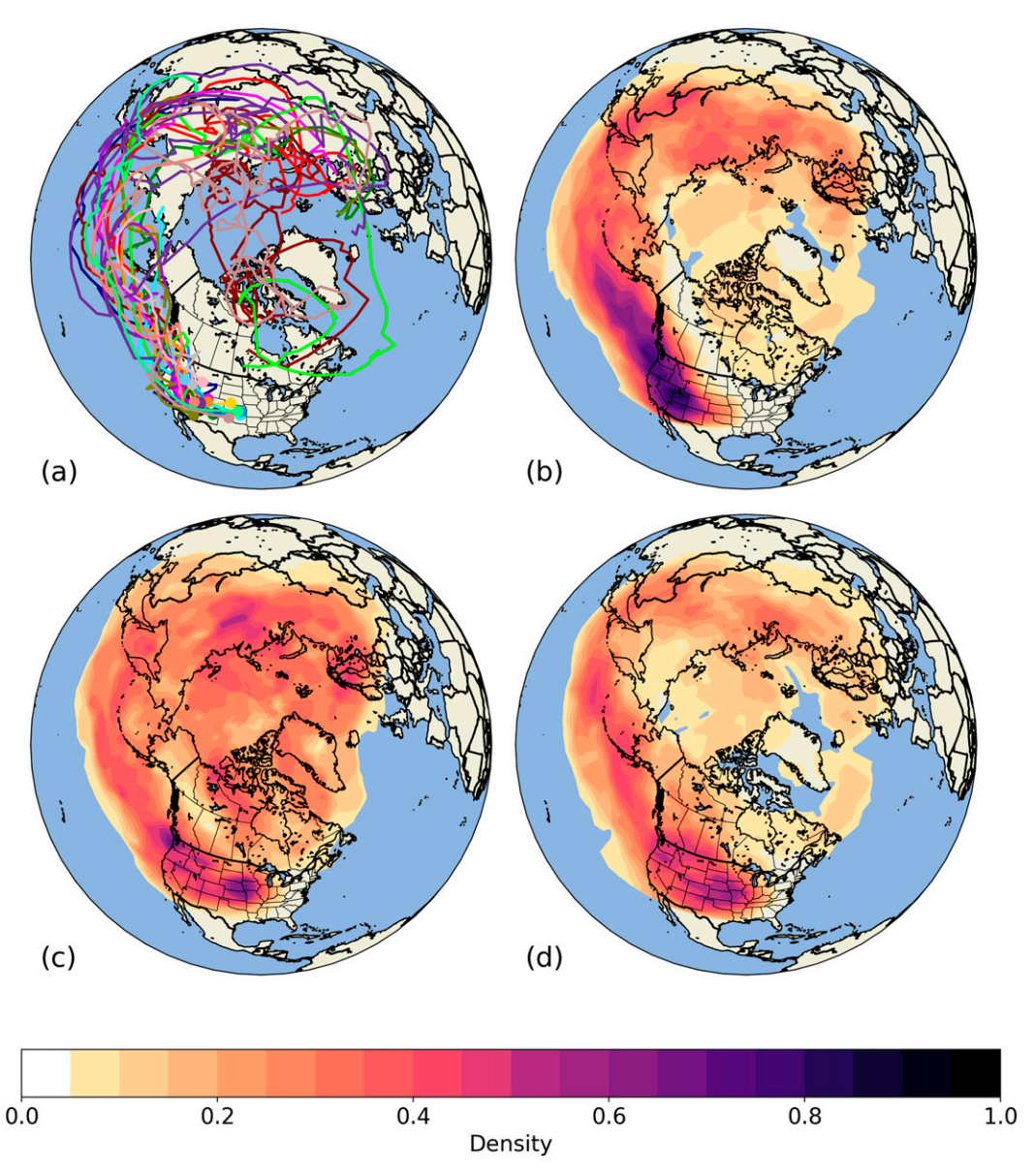


FIG. 6. (a) Tracks of the 21 PV anomalies most closely associated with each case in the Oklahoma cluster. The location of the vortex at the time of the outbreak is indicated with a colored circle at the end of each track. (b) A probability density map of the tracks in (a), calculated as the probability of any anomaly in the cluster passing within 555 km of a location. (c) As in (b), but for the vortex tracks of the 15 Illinois cases. (d) As in (b), but for the vortex tracks of the 27 Alabama cases.

PV anomalies from all three clusters have significantly stronger anomalies and circulations, reach substantially lower latitudes, and are longer-lived than typical TPVs (Fig. 7). Statistical significance is established using the two-sided Kolmogorov–Smirnov (K–S) test (Massey 1951), along with a t test for the mean, and all cluster distributions are found to be statistically different from the full TPV record at p < 0.05. On the other hand, the vortices associated with tornado event clusters are slightly less distinguishable from a typical tropospheric PV anomaly with no latitude requirement. Significant differences between the cluster cases and average PV anomalies are

detected in anomaly strength and minimum latitude, while differences in circulation (aside from the Oklahoma cluster) and lifetime are not found to be significant.

For cluster cases, maximum tropopause potential temperature anomalies average between -30 and -40 K, while the average falls around -20 K for the full record of TPVs and just under -30 K for the full PV anomaly record (Fig. 7a). Vortices within each cluster move more southward than either typical TPVs or PV anomalies, reaching as far south as 25°N for those associated with the Alabama cluster (Fig. 7b). Circulation distributions peak around 75–175 m² s⁻¹ for the three clusters

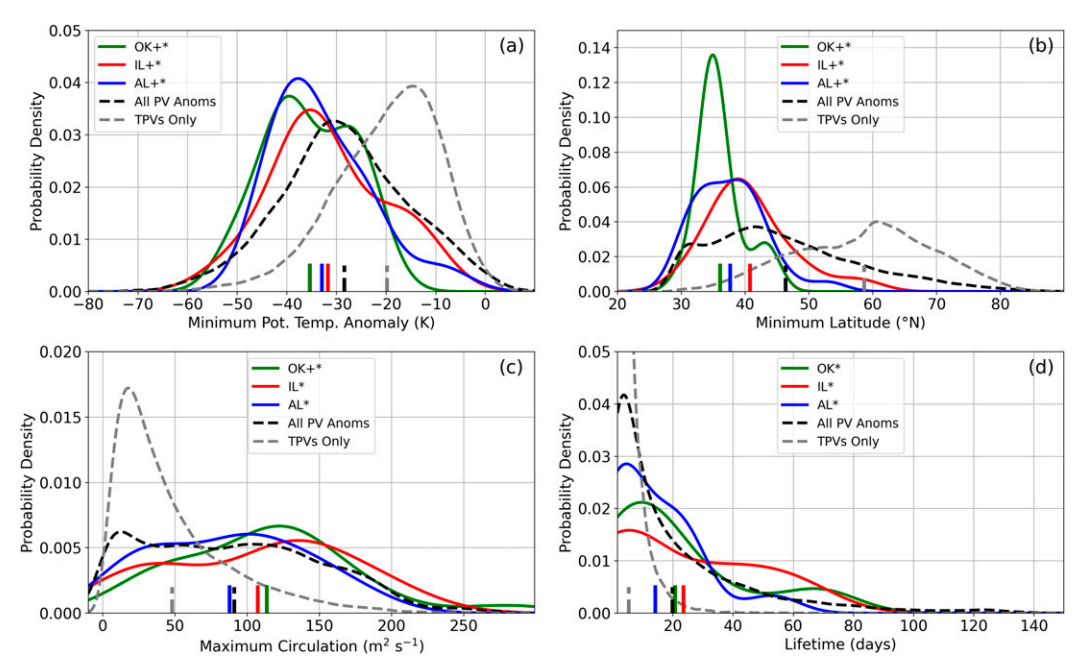


FIG. 7. Vortex property distributions of (a) minimum potential temperature anomaly (K; calculated against a 1981–2010 climatology), (b) minimum latitude (°N), (c) maximum circulation ($m^2 s^{-1}$), and (d) lifetime (days). The dashed black contours represent a random sample ($n=10\,000$) of all PV anomalies, processed through the split detection algorithm described in the text, while the dashed gray contours represent the distribution of TPVs only. The green, red, and blue contours represent the Oklahoma, Illinois, and Alabama clusters, respectively. Vertical lines at the bottom of each panel represent the mean value of the corresponding distribution. A + symbol in the legend represents significance at the 95% level with respect to the full PV anomaly distribution, determined using Kolmogorov–Smirnov and t tests. A * symbol represents statistical significance calculated the same way with respect to the TPV tracks only.

in contrast to less than $50\,\mathrm{m}^2\,\mathrm{s}^{-1}$ in the full record of TPVs (Fig. 7c). The full PV anomaly record, however, produces and average of around $100\,\mathrm{m}^2\,\mathrm{s}^{-1}$, much closer to the cluster averages. So, while the cluster vortices produce stronger attendant flow than an average Arctic-originating vortex, this flow is not necessarily stronger than an average midlatitude PV anomaly. Similarly, outbreak vortex lifetimes, sometimes exceeding two months in all three clusters, are significantly longer than average TPV lifetimes, but only marginally longer than average PV anomaly lifetimes (Fig. 7d). These results strongly suggest an association of tornado outbreaks with long-lived, intense PV anomalies, a pattern that may prove useful in forecasting applications.

The vortices associated with tornadic events exhibit a clear pattern of meridional motion with time, which may be especially useful for forecasting applications. Arctic-originating anomalies tend to slowly descend from high latitudes in the weeks preceding an outbreak (Fig. 8a). Around a week prior to the event, these TPVs, now in the same pathway as anomalies that form south of 60°N, begin to move eastward at a constant latitude of around 50°N before rapidly descending into the continental United States around 3 days before the outbreak (Fig. 8a). During this equatorward journey, the vortices retain roughly constant intensity compared to climatology until their final descent. At this point, potential temperature anomalies

rapidly drop as the vortices contrast sharply with the climatologically warmer conditions in the midlatitudes, then increase as the vortices are sheared apart by the jet (Fig. 8b). This decrease in anomalies is less defined for the Illinois cluster, where the relatively high latitudes of the vortices may lessen the anomalies. On the other hand, vortex circulations gradually increase leading up to the outbreak (Fig. 8c). Coupled with nearly constant vortex radii, this indicates an increase in vortex strength in the days before the outbreak (Fig. 8d). However, in the Illinois and Alabama clusters in particular, vortex circulations and radii decrease quickly upon descent into the United States (Figs. 8c,d). These decreases coincide with increases in potential temperature anomaly and are most likely reflective of the dissipation of these vortices. It is also of note that most of the PV anomalies maintain radii of several hundred kilometers back to their supposed genesis points, which may imply that these vortices originated from further splits that were not picked up by the tracking algorithm (Fig. 8d). Further, the case study presented above generally agrees with this average vortex evolution pattern, indicating that the case study is a good representation of the vortices under consideration (Fig. 5).

The presence of PV anomaly–jet streak couplets west of the outbreak regions is evident in composite anomalies starting 36 h prior to the start of the event up to the approximate time of the outbreak (Fig. 9). While divided composites are not

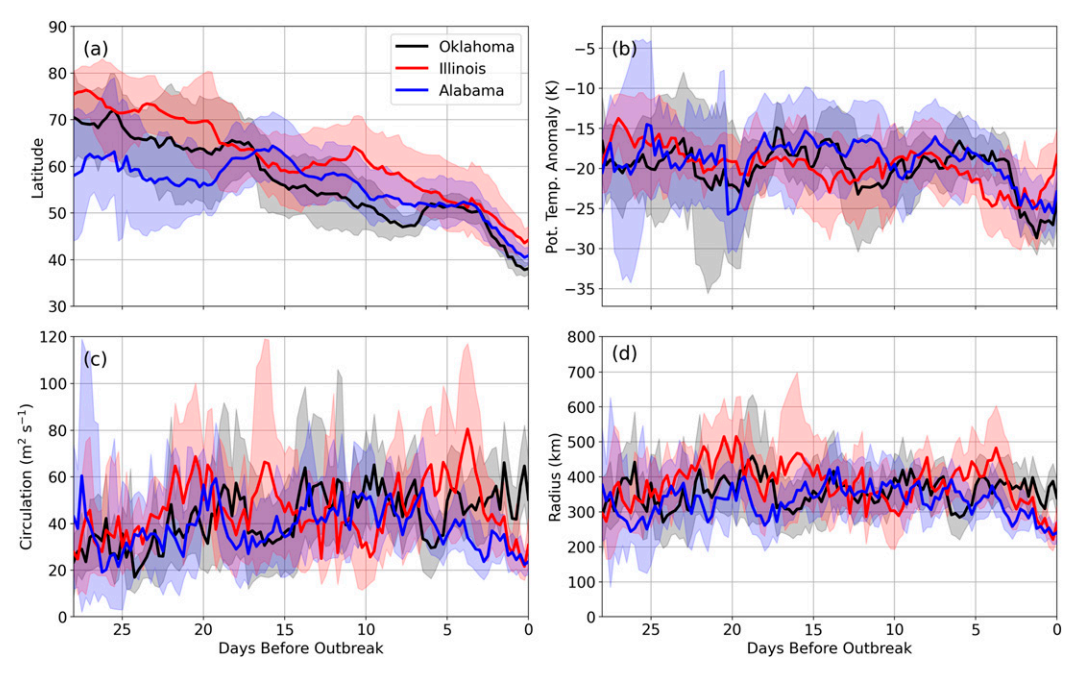


FIG. 8. (a) Cluster-average vortex latitude (solid lines) as a function of the number of days prior to the tornado outbreak for each cluster. Shading indicates a 95% confidence interval, determined using bootstrap resampling. (b) As in (a), but for cluster-average vortex potential temperature anomaly (K). (c) As in (a), but for cluster-average vortex circulation $(m^2 s^{-1})$. (d) As in (a), but for cluster-average vortex radius (km).

included here, we note that although especially large outbreak events exhibit slightly different patterns than the smaller events, they do not seem to dominate or bias the magnitude of these composites. For the Oklahoma cluster, an average anomaly signal (identified by closed contours of anomalously low tropopause potential temperature values) is apparent moving across southern Oregon 36 h before the event time, and over the Colorado Plateau region by the time of convection. An averaged jet maximum is present to the south of the vortex at both time steps and eventually orients with its exit region nearly over central Oklahoma at the time of the outbreak, as would be expected from the theoretical model of jet streaks and severe weather (Figs. 9a,b). In the Oklahoma cases only, a slight second jet maximum is present to the south, over northern Mexico. This is likely indicative of a subtropical jet present in some cases. So, the subtropical jet may play a role in jet streak development along with the circulation about the PV anomaly (known as the Arctic jet when the anomaly is a TPV, e.g., Shapiro et al. (1987), but the relatively southward position of this jet maximum indicates that this may not be as consistent of a factor (Figs. 9a,b).

The Illinois and Alabama clusters display similar patterns (Figs. 9c-f). In general, the Illinois anomaly signal is weaker, perhaps due to a longer period spent by the vortex in the midlatitudes on account of the more southerly track (Figs. 6c and 9c,d). The average anomaly moves eastward from over the western United States, reaching northeastern Colorado at the time of the outbreak. The jet streak south of the vortex follows a similar path (Figs. 9c,d). Similarly, the average Alabama PV anomaly moves from western Colorado to the

central Great Plains, along with the corresponding average jet streak (Figs. 9e,f). The Illinois and Alabama clusters also exhibit a second jet streak feature northeast of the event area, which, while likely not directly related to the vortex of interest, could also contribute to the synoptic forcing. It is important to note, however, that as in the case study, the composite tropopause flow near all three outbreak regions is curved (Figs. 9b,d,f). Hence, regions of forcing for ascent may not line up exactly with the four-quadrant conceptual model, though they are still expected to be located near the jet exit region. Although the exact orientations of the PV anomaly and jet streak relative to the outbreak vary from event to event, a majority of the cases include a PV anomaly-jet pair of some form. Across all three clusters, 21 cases (out of 63 total) did not exhibit a clear anomaly-jet streak couplet in the vicinity of the tornado outbreak. In these cases, the nearby PV anomalies (as discussed and tracked above) may not have had an effect on the outbreak or may have influenced the synoptic environment in an indirect manner (i.e., by altering the large-scale flow from afar).

c. Synoptic-scale shear, vertical motion forcing, and static stability

Although a persistent TPV-jet streak signature is present across the majority of cases in all three clusters, it remains to be shown that these events included a significant synoptic forcing. Regions of significantly elevated wind shear are evident across virtually the entire outbreak region of all three clusters (Figs. 10a-c). These regions of increased shear can be tied back directly to the jet streak patterns discussed in section 3b,

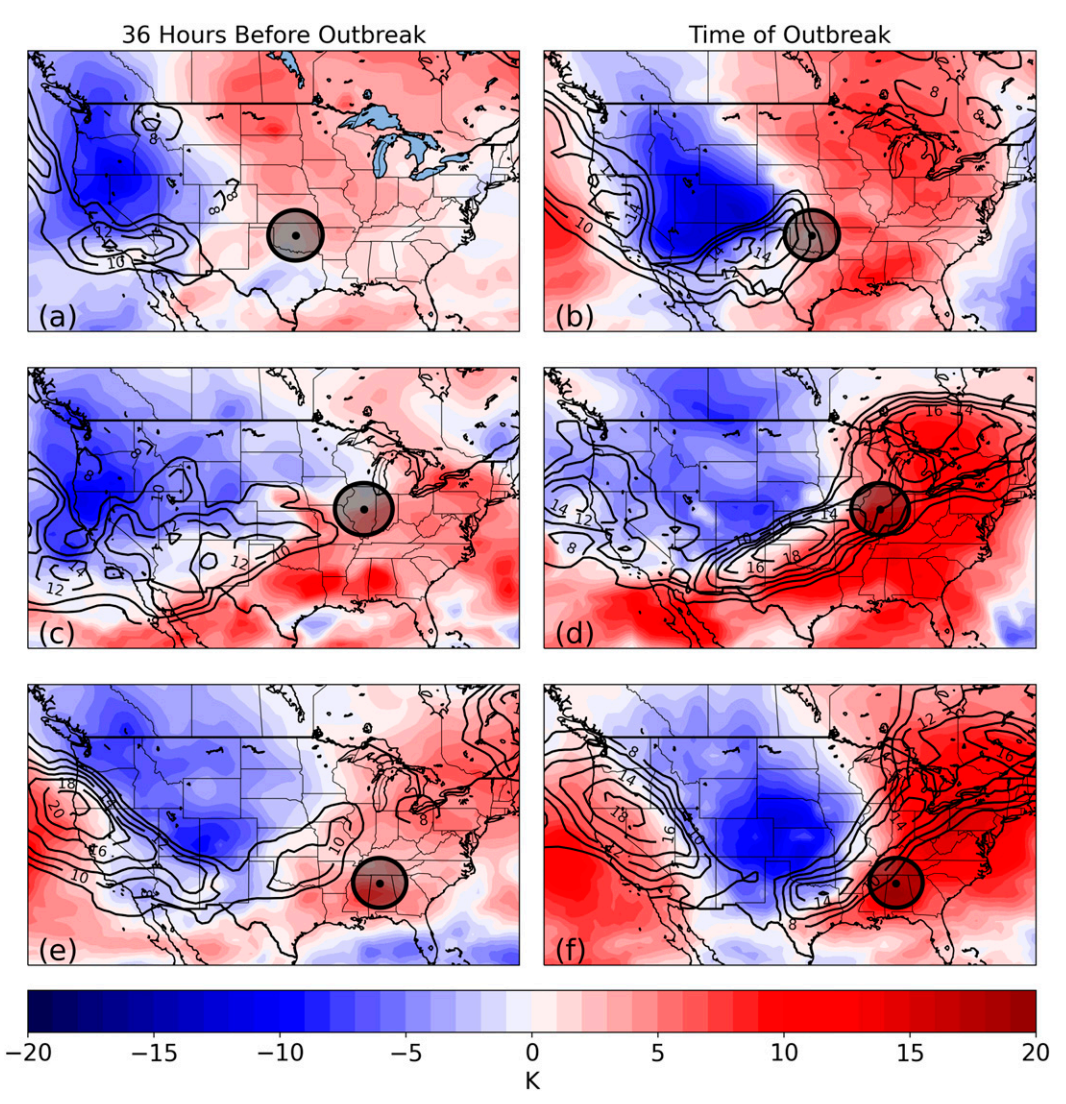


FIG. 9. (a) Composite anomalies of tropopause potential temperature (fill; K) and tropopause wind speeds (contour; m s $^{-1}$) over the Oklahoma cluster cases, 36 h before the tornado event. (b) As in (a), but composited at the time of each event. (c) As in (a), but for the Illinois cluster. (d) As in (b), but for the Illinois cluster. (e) As in (a), but for the Alabama cluster. (f) As in (b), but for the Alabama cluster. The regions of radius 300 km defining each cluster used in the analysis are shown in black.

demonstrating the importance of the jet streak in generating the large-scale shear needed for tornadic events. In each cluster, there is a clear pattern of quasigeostrophic forcing for ascent over the area of the outbreak, as calculated using all three terms of the right-hand side of Eq. (1). The region of ascent is well-aligned with the tornado locations in the Oklahoma and Alabama clusters (Figs. 10d,f). Across the Illinois region, the area of ascent is slightly north and east of the cluster center (Fig. 10e). This variation could be attributed to the relative positions of each outbreak within the cluster. The regions of significance also line up well with the outbreak locations, indicating that these regions are seeing significantly more forcing for vertical motion at the time of the outbreak than climatologically (Figs. 10d-f). We also note significant regions of enhanced

ascent north of the outbreak regions across all three clusters (Fig. 10). Many tornado events occur in the warm sector of midlatitude cyclones, which would be centered near these regions of enhanced ascent. Thus, it is possible that ageostrophic forcing from the jet streak may strengthen a surface cyclone, thereby increasing moisture flux into the outbreak region and intensifying surface boundaries. This provides an additional indirect pathway whereby the jet streak forcing could influence the severe storm environment.

All three clusters also exhibit a pattern of anomalously low static stability in the midatmospheric layer above the outbreak zone (Figs. 10g-i). This signal is generally much broader than the relatively narrow areas of ascent, covering the entire outbreak region in the Oklahoma and Alabama clusters, and

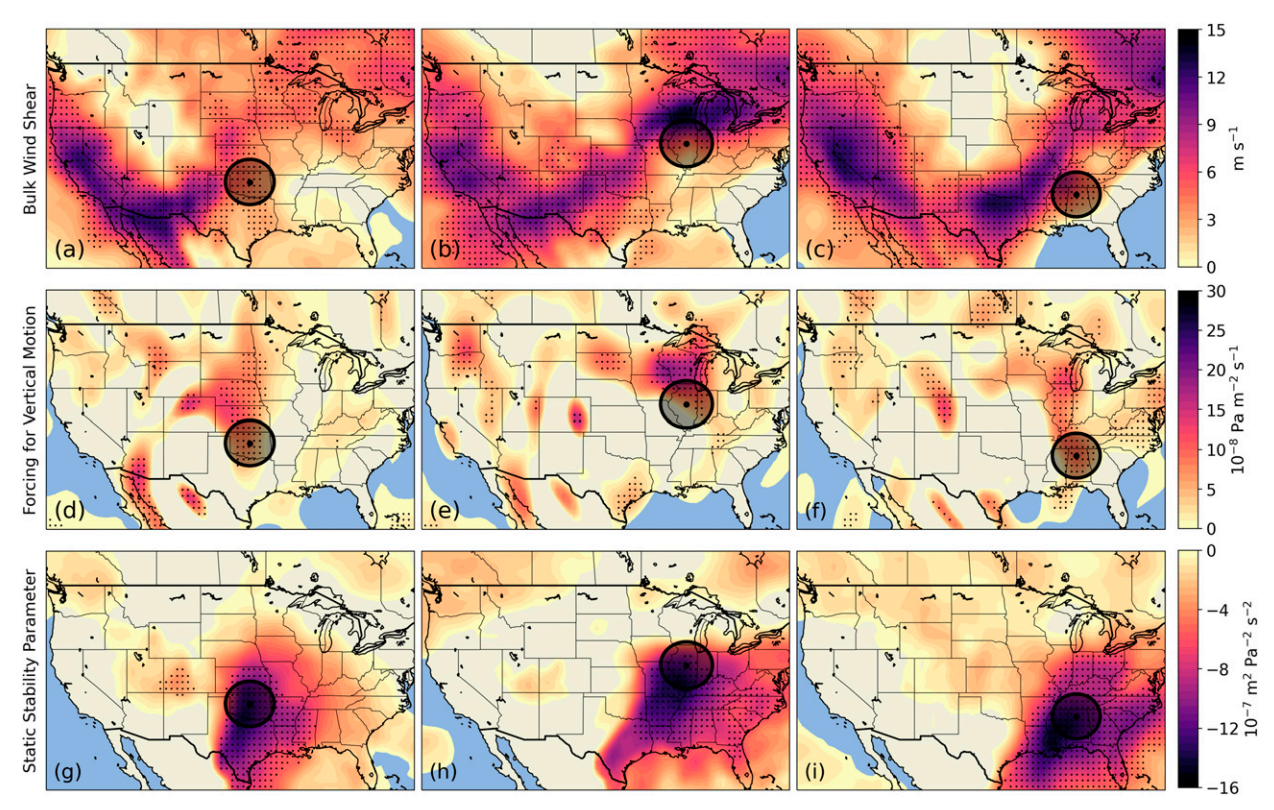


Fig. 10. (a) Composite anomalies of 900–500-hPa bulk wind shear for Oklahoma cluster cases at the approximate time of the outbreak (m s⁻¹). Stippling indicates significance at the global 95% level determined using a one-tailed t test and a false discovery rate analysis of field significance, and only positive anomalies are shown. (b) As in (a), but for the Illinois cluster. (c) As in (a), but for the Alabama cluster. (d) As in (a), but for vertical motion forcing at 700 hPa, calculated using the complete right-hand side of the Trenberth QG omega equation ($10^9 \, \text{Pa} \, \text{m}^{-2} \, \text{s}^{-1}$). (e) As in (d), but for the Illinois cluster. (f) As in (d), but for the Alabama cluster. (g) As in (a), but for the static stability parameter at 700 hPa ($10^7 \, \text{m}^2 \, \text{Pa}^{-2} \, \text{s}^{-2}$). Only negative values are shown. (h) As in (g), but for the Illinois cluster. (i) As in (g), but for the Alabama cluster. The regions of radius 300 km defining each cluster used in the analysis are shown in black.

almost the entire Illinois region. The regions of statistical significance are also broad, covering each outbreak region almost entirely. This decrease in static stability relative to climatology could, especially in the cases with collocated vortices, be related to the anomalously cold upper troposphere conditions associated with these PV anomalies. As a whole, all three of these synoptic signals are indicative of tornadic environments, and all three can be theoretically associated with the TPV–jet streak feature to some degree. Since the enhanced shear is the most direct link, it likely explains the majority of the relationship.

d. Comparison of null cases and tornadic cases

Among the full slate of TPV passages through the United States examined in the second part of this study, the vast majority were not associated with any tornado events. Indeed, only 10%, 6%, and 5% of TPVs passing near the Oklahoma, Illinois, and Alabama cluster regions, respectively, occurred synchronously with any tornado activity. The primary explanation for these low percentages is seasonality. A large proportion of TPV passages through the United States occur during the winter, when other environmental factors, such as a

lack of low-level moisture, may prohibit severe storm activity despite the enhanced synoptic forcing provided by the TPV. Indeed, the majority of TPV-tornado events across all three clusters occur during the spring, while null cases (a TPV passage without tornado activity) occur much more often in the winter months (Fig. 11a). The Alabama and Illinois clusters also exhibit elevated probabilities of TPV-tornado cases in the winter and summer, respectively, in general alignment with tornado climatologies in those regions.

TPV passages during the spring are especially apt to contribute to tornado events due to the overlapping presence of shear and low-level moisture during this period. In all three cluster regions, wind shear maximizes during the winter and minimizes during the summer, while dewpoint temperatures follow the opposite trend (Figs. 11b-c). So, the spring generally provides the best balance of shear and moisture for tornadic events. It is also clear that regardless of season, TPV-tornado cases occur in more humid environments than their null case counterparts, as will be explored further below (Fig. 11c). In short, the vast majority of TPV null cases can be explained by timing; the TPV must be present at a time when adequate environmental shear and moisture are present for there to be

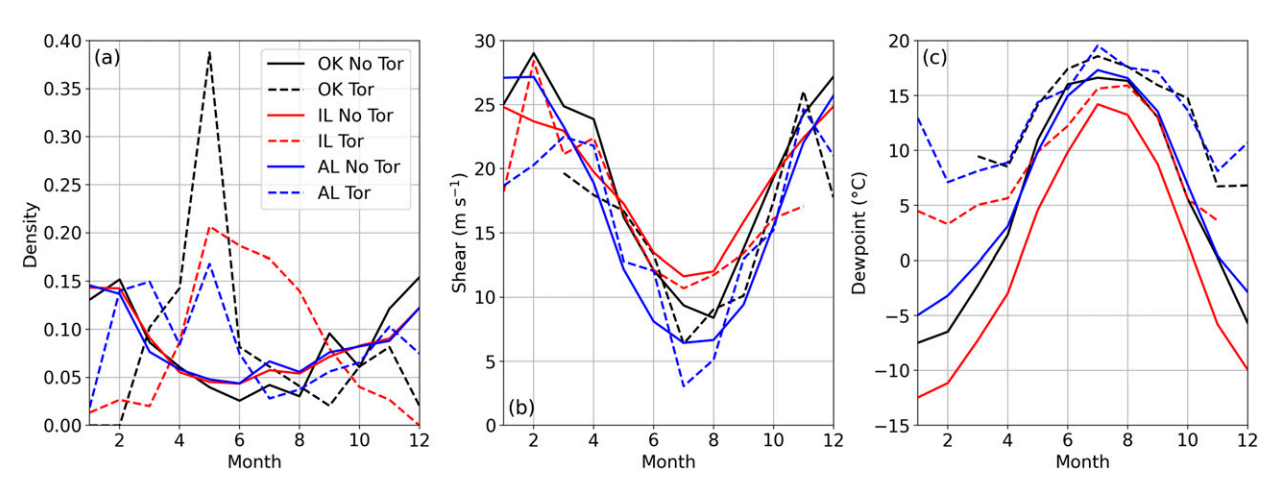


FIG. 11. (a) Monthly line-histograms of TPV occurrences within the null case search area for cases with (dashed lines) and without (null cases, solid lines) tornadoes for the Oklahoma (black), Illinois (red), and Alabama (blue) clusters. (b) Mean monthly 900–500-hPa wind shear (m s⁻¹) averaged over the 300-km radius cluster area for all non-tornado (null; solid lines) and tornado (dashed lines) cases. (c) As in (b), but for mean monthly 925-hPa dewpoint temperature (°C).

any chance of a tornado event. Still, even during the spring, a minority of TPVs over the United States are associated with tornado activity.

To investigate these remaining null cases, we attempt to filter out seasonal influences and spatial variations in TPV location using weighted averaging. For the Oklahoma cluster, both the null case composite and tornado case composite include a clear surface cyclone to the west of the outbreak region, along with a dryline near the Texas-Oklahoma border (Figs. 12a,b); however, in the null cases, these features are notably weaker. In addition, positive dewpoint anomalies are much higher over the outbreak region during the tornado cases, likely as a result of enhanced northward moisture flux from the more developed cyclone (Figs. 12a,b). The Illinois and Alabama regions exhibit similar patterns. The tornado composites include strong surface cyclones over the upper Midwest with associated frontal boundaries moving toward the respective outbreak regions, along with positive moisture anomalies across the areas of interest (Figs. 12c-f). The null cases, on the other hand, show a more progressive surface pattern in which the cyclone has moved northeast, leaving the outbreak regions dry and behind potential lifting mechanisms (Figs. 12c-f). As a whole, null cases seem to occur when the upper level features (i.e., the TPV) are temporally or spatially out of phase with the surface features (i.e., the surface cyclone and associated moisture fluxes and lifting mechanisms). As hypothesized then, TPVs and other upper-level PV anomalies alone are not sufficient to produce tornado outbreaks. Rather, they provide an additional synoptic forcing to environments already primed for severe storms.

4. Summary and discussion

Using archived tornado data, this study identified several clusters of recurrent tornado activity across the United States, and, within these clusters, identified multiple significant tornado outbreaks for further study. Across all three clusters and

63 cases of tornado activity studied, we identified a persistent PV anomaly-jet streak pattern to the west of the region of convection and a jet exit region collocated with thunderstorm occurrence. Dependent on the cluster, a slight majority of these anomalies could be traced back to the Arctic, thereby qualifying as TPVs, while the remainder formed over the North Pacific. The individual vortices associated with each outbreak followed a similar path into the United States, traveling across the North Pacific before dropping southward along the west coast of North America. These vortices were found to be significantly more anomalous and slightly longer-lived than average, suggesting that these outbreak-related TPVs may share some common characteristics. Moreover, these PV anomalies followed a predictable pattern of movement in the week preceding the outbreak, dropping rapidly southward around 3 days prior to the tornadic event.

Statistically significant patterns of enhanced bulk wind shear, quasigeostrophic forcing for ascent, and low static stability in the middle atmosphere were present over the outbreak area in all three clusters. The theoretical physical linkages between TPVs and these synoptic forcings indicate the potential for a causal relationship between TPVs and tornado outbreaks, but that relationship was not examined herein. Examining a separate dataset of all TPV passages near the cluster regions, we find that while the majority of TPVs are not associated with tornado events, those vortices that are exhibit clear seasonal and spatial trends. TPV-tornado cases happen predominately in the spring when both shear and low-level moisture are present in sufficient amounts, while null cases occur mostly during the winter, when factors such as low humidity and high stability prohibit widespread severe storm activity. TPVs that are associated with tornado events also tend to align spatially and temporally with surface features, including surface fronts and regions of surface moisture.

As in several previous observational (Bluestein and Thomas 1984; Sanders and Blanchard 1993) and climatological (Rose et al. 2004; Clark et al. 2009) studies, the present study found

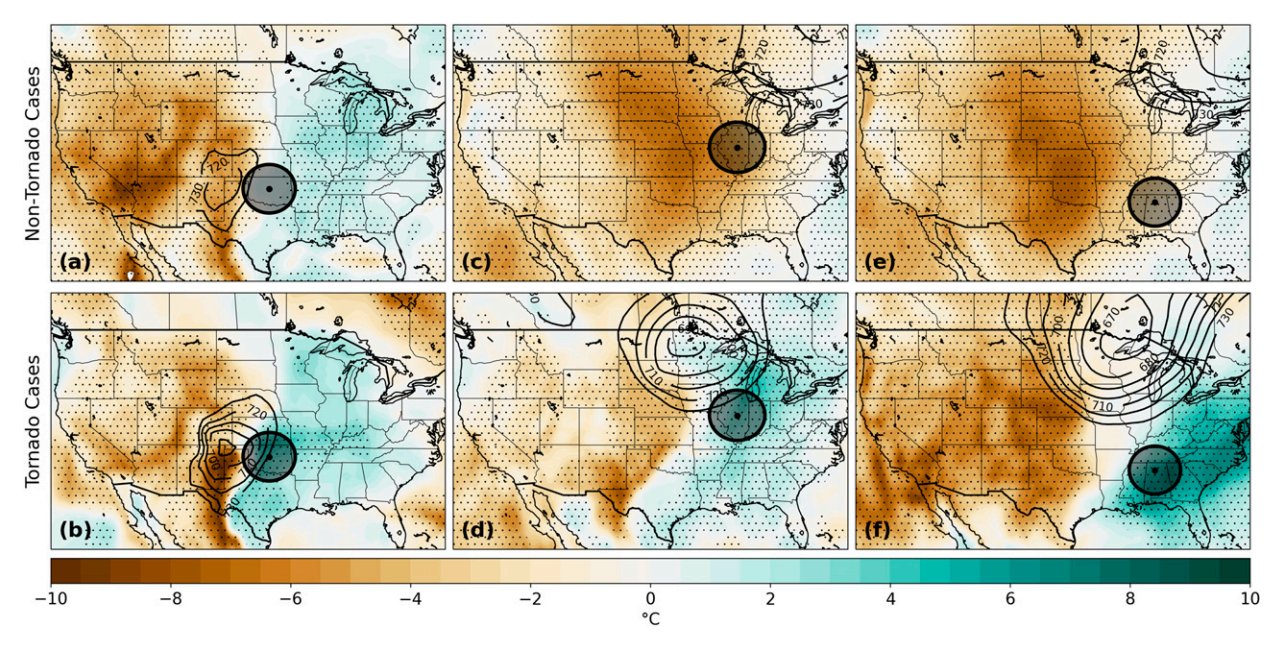


FIG. 12. (a) Temporally and spatially weighted mean 925-hPa dewpoint temperature anomaly (fill; C) and 925-hPa geopotential heights (contours; m) for non-tornado (null) Oklahoma TPV cases. (b) As in (a), but for Oklahoma TPV cases with tornado reports. (c) As in (a), but for the Illinois cluster. (d) As in (b), but for the Illinois cluster. (e) As in (a), but for the Alabama cluster. (f) As in (b), but for the Alabama cluster. The regions of radius 300 km defining each cluster used in the analysis are shown in black. Stippling indicates significance at the global 95% level determined using a two-tailed *t* test and a false discovery rate analysis of field significance.

tornado events to be commonly (though not always) associated with the presence of an upper-level jet streak, with storms occurring most often in the right exit region (note, once again, that the four-quadrant model is not perfectly applicable in these curved flow regimes). In total, 42 of the 63 (67%) primary cases studied followed this pattern, while the remaining outbreaks occurred without a clear jet streak influence. The jet maxima in these 42 cases helped create environments conducive to tornado outbreaks by increasing deep-layer shear, enhancing large-scale ascent via quasigeostrophic forcing, and potentially working to lower atmospheric static stability, as numerous previous studies have also indicated (Bluestein and Thomas 1984; Sanders and Blanchard 1993; Uccellini and Johnson 1979). It is important to reiterate, however, that the jet streaks in these cases served only to bolster tornadic potential in environments that already included other well established severe weather prerequisites like moisture and surface lifting mechanisms (Weisman and Klemp 1982; Johns and Doswell 1992; Doswell et al. 1996).

Most of the cases studied (including all of the 42 jet streak cases) were associated with a tropopause PV anomaly that may have played a role in the localized strengthening of the jet and amplification of the wave pattern over North America (Hakim 2000; Pyle et al. 2004). Such vortices have been shown to initiate jet maxima in the past (Simmonds and Rudeva 2014; Cavallo and Hakim 2010; Winters and Martin 2017); however, for the first time, this work showed that the jet streak-generating PV anomalies associated with tornado outbreaks are often Arctic in origin. Moreover, these Arctic-originating TPVs (along with non-TPV vortices which form in the Northern

Pacific) follow a common pathway into the midlatitudes during the week preceding the tornado outbreaks. This recurrent TPV trajectory may have benefits for severe weather forecasting, particularly over time scales of longer than a few days. For instance, the presence of a strong TPV or other PV anomaly over the Gulf of Alaska several days prior to a possible tornado outbreak may indicate the potential for a particularly strong tornado event. In short, it seems that TPVs advected toward the midlatitudes could signal a higher risk of widespread severe storms, though a more comprehensive and quantitative future study is needed to support this conjecture.

It is also essential to note some of the limitations of this PV anomaly framework, especially as it relates to null events. We have shown in this study that PV anomalies (commonly Arctic in origin) are often present during tornado outbreaks, along with regions of enhanced wind shear and forcing for ascent, which may be related to vortex–jet streak dynamics. However, as was illustrated in section 3d, TPVs and similar anomalies alone are not enough to facilitate a tornado event if other necessary features are not in place. Likewise, tornado outbreaks do not require a PV anomaly–jet streak pattern to occur. Indeed, 21 of the 63 significant tornado outbreaks studied possessed no such signal. Instead, PV anomalies are hypothesized to provide an additional synoptic forcing to environments already favorable for tornado outbreaks, a connection that will need to be more definitively proven in future studies.

Although this work has demonstrated a preliminary linkage between TPVs and tornado events, future experiment-based studies should serve to confirm and quantify this connection. For instance, numerical simulations in which TPVs are weakened or removed entirely (via piecewise PV inversion) prior to the onset of severe weather could more precisely demonstrate the impact of the vortex on the severe weather environment. Similarly, future studies should more extensively investigate how tornado outbreaks are linked with the characteristics of the associated TPV, perhaps through an ensemble sensitivity analysis. Additional work is also needed to determine the genesis mechanisms for these vortices and investigate the exact flow characteristics that cause them to descend equatorward. Moreover, the extension of previous work on PV anomaly jet strengthening and jet superpositions to directly examine TPVs and Arctic-polar jet superpositions may more fully elucidate the physics of many of the cases presented here. Each of these future steps would greatly improve the forecasting utility of this work by providing information on how PV anomalies may be expected to affect tornado outbreaks and improving the ability to forecast these events well in advance.

Acknowledgments. We thank the members of the University of Oklahoma Arctic and Antarctic Atmospheric Research Group for their advice and support. This work was supported under Office of Naval Research Grant N00014-16-1-2489 and is based on work supported by the National Science Foundation Graduate Research Fellowship Program under Grant 105411900. Any opinions, findings, and conclusions or recommendations expressed in this material are those of the author(s) and do not necessarily reflect the views of the National Science Foundation.

Data availability statement. Tornado report data from the SPC may be downloaded online at https://www.spc.noaa.gov/wcm/#data. ERA-Interim data may be obtained from https://www.ecmwf.int/en/forecasts/datasets/archive-datasets/reanalysis-datasets/era-interim.

REFERENCES

- Barrett, B. S., and V. A. Gensini, 2013: Variability of central United States April–May tornado day likelihood by phase of the Madden–Julian oscillation. *Geophys. Res. Lett.*, 40, 2790– 2795, https://doi.org/10.1002/grl.50522.
- Beebe, R., and F. C. Bates, 1955: A mechanism for assisting in the release of convective instability. *Mon. Wea. Rev.*, **63**, 1–10, https://doi.org/10.1175/1520-0493(1955)083<0001: AMFAIT>2.0.CO;2.
- Bluestein, H. B., 1992: Synoptic-Dynamic Meteorology in Midlatitudes. Vol. I: Principles of Kinematics and Dynamics, Oxford University Press, 349 pp.
- —, and K. W. Thomas, 1984: Diagnosis of a jet streak in the vicinity of a severe weather outbreak in the Texas Panhandle. Mon. Wea. Rev., 112, 2499–2520, https://doi.org/10.1175/1520-0493(1984)112<2499:DOAJSI>2.0.CO;2.
- Bosart, L. F., G. J. Hakim, K. R. Tyle, M. A. Bedrick, W. E. Bracken, M. J. Dickinson, and D. M. Schultz, 1996: Large-scale conditions associated with the 12–14 March 1993 cyclone ("Superstorm '93") over eastern North America. *Mon. Wea. Rev.*, 124, 1865–1891, https://doi.org/10.1175/1520-0493(1996) 124<1865:LSACAW>2.0.CO;2.
- Cavallo, S. M., and G. J. Hakim, 2009: Potential vorticity diagnosis of a tropopause polar cyclone. *Mon. Wea. Rev.*, 137, 1358– 1371, https://doi.org/10.1175/2008MWR2670.1.

- —, and —, 2010: Composite structure of tropopause polar cyclones. *Mon. Wea. Rev.*, **138**, 3840–3857, https://doi.org/ 10.1175/2010MWR3371.1.
- —, and —, 2012: Radiative impact on tropopause polar vortices over the Arctic. *Mon. Wea. Rev.*, **140**, 1683–1702, https://doi.org/10.1175/MWR-D-11-00182.1.
- —, and —, 2013: Physical mechanisms of tropopause polar vortex intensity change. J. Atmos. Sci., 70, 3359–3373, https:// doi.org/10.1175/JAS-D-13-088.1.
- Clark, A. J., C. J. Schaffer, W. A. Gallus Jr., and K. Johnson-O'Mara, 2009: Climatology of storm reports relative to upper-level jet streaks. Wea. Forecasting, 24, 1032–1051, https://doi.org/10.1175/2009WAF2222216.1.
- Cook, A. R., and J. T. Schaefer, 2008: The relation of El Niño–Southern Oscillation (ENSO) to winter tornado outbreaks. *Mon. Wea. Rev.*, 136, 3121–3137, https://doi.org/10.1175/2007MWR2171.1.
- —, L. M. Leslie, D. B. Parsons, and J. T. Schaefer, 2017: The impact of El Niño–Southern Oscillation (ENSO) on winter and early spring U.S. tornado outbreaks. *J. Appl. Meteor. Climatol.*, 56, 2455–2478, https://doi.org/10.1175/JAMC-D-16-0249.1.
- Dee, D. P., S. M. Uppala, A. J. Simmons, P. Berrisford, P. Poli, S. Kobayashi, and P. Bechtold, 2011: The ERA-Interim reanalysis: Configuration and performance of the data assimilation system. *Quart. J. Roy. Meteor. Soc.*, 137, 553–597, https://doi.org/10.1002/qj.828.
- Doswell, C. A., S. J. Weiss, and R. H. Johns, 1993: Tornado forecasting: A review. *The Tornado: Its Structure, Dynamics, Prediction, and Hazards*, C. Church et al., Eds., Amer. Geophys. Union, 557–571.
- —, H. E. Brooks, and R. A. Maddox, 1996: Flash flood forecasting: An ingredients-based methodology. Wea. Forecasting, 11, 560–581, https://doi.org/10.1175/1520-0434(1996)011<0560:FFFAIB>2.0.CO:2.
- Gensini, V. A., and A. Marinaro, 2016: Tornado frequency in the United States related to global relative angular momentum. Mon. Wea. Rev., 144, 801–810, https://doi.org/10.1175/MWR-D-15-0289.1.
- —, D. Gold, J. T. Allen, and B. S. Barrett, 2019: Extended U.S. tornado outbreak during late May 2019: A forecast of opportunity. *Geophys. Res. Lett.*, 46, 10 150–10 158, https://doi.org/10.1029/2019GL084470.
- ——, B. S. Barrett, J. T. Allen, D. Gold, and P. Sirvatka, 2020: The Extended-Range Tornado Activity Forecast (ERTAF) project. *Bull. Amer. Meteor. Soc.*, **101**, E700–E709, https://doi.org/ 10.1175/BAMS-D-19-0188.1.
- Hakim, G. J., 2000: Climatology of coherent structures on the extratropical tropopause. *Mon. Wea. Rev.*, **128**, 385–406, https://doi.org/10.1175/1520-0493(2000)128<0385:COCSOT>2.0.CO;2.
- —, and A. K. Canavan, 2005: Observed cyclone–anticyclone tropopause vortex asymmetries. *J. Atmos. Sci.*, **62**, 231–239, https://doi.org/10.1175/JAS-3353.1.
- —, L. F. Bosart, and D. Keyser, 1995: The Ohio valley wavemerger cyclogenesis event of 25–26 January 1987. Part I: Multiscale case study. *Mon. Wea. Rev.*, **123**, 2663–2692, https://doi.org/10.1175/1520-0493(1995)123<2663:TOVWMC> 2.0.CO;2.
- —, D. Keyser, and L. F. Bosart, 1996: The Ohio valley wave-merger cyclogenesis event of 25–26 January 1987. Part II: Diagnosis using quasigeostrophic potential vorticity inversion. *Mon. Wea. Rev.*, **124**, 2176–2205, https://doi.org/10.1175/1520-0493(1996)124<2176:TOVWMC>2.0.CO;2.

- Johns, R. H., and C. A. Doswell, 1992: Severe local storms fore-casting. Wea. Forecasting, 7, 588–612, https://doi.org/10.1175/1520-0434(1992)007<0588:SLSF>2.0.CO;2.
- Massey, F. J., Jr., 1951: The Kolmogorov–Smirnov test for goodness of fit. J. Amer. Stat. Assoc., 46, 68–78, https://doi.org/10.1080/01621459.1951.10500769.
- Mercer, A. E., C. M. Shafer, and C. A. Doswell, 2012: Synoptic composites of tornadic and nontornadic outbreaks. *Mon. Wea. Rev.*, 140, 2590–2608, https://doi.org/10.1175/MWR-D-12-00029.1.
- Miller, D. E., Z. Wang, R. J. Trapp, and D. S. Harnos, 2020: Hybrid prediction of weekly tornado activity out to week 3: Utilizing weather regimes. *Geophys. Res. Lett.*, 47, e2020GL087253, https://doi.org/10.1029/2020GL087253.
- Moore, J. T., and G. E. VanKnowe, 1992: The effect of jet-streak curvature on kinematic fields. *Mon. Wea. Rev.*, **120**, 2429–2441, https://doi.org/10.1175/1520-0493(1992)120<2429: TEOJSC>2.0.CO;2.
- Moore, T. W., and M. P. McGuire, 2020: Tornado-days in the United States by phase of the Madden–Julian oscillation and global wind oscillation. *Climate Dyn.*, **54**, 17–36, https://doi.org/10.1007/s00382-019-04983-y.
- Morgan, M. C., and J. W. Nielson-Gammon, 1998: Using tropopause maps to diagnose midlatitude weather systems. *Mon. Wea. Rev.*, 126, 2555–2579, https://doi.org/10.1175/1520-0493(1998)126<2555: UTMTDM>2.0.CO;2.
- Peters, D., and D. W. Waugh, 1996: Influence of barotropic shear on the poleward advection of upper-tropospheric air. *J. Atmos. Sci.*, **53**, 3013–3031, https://doi.org/10.1175/1520-0469(1996) 053<3013:IOBSOT>2.0.CO;2.
- Pyle, M. E., D. Keyser, and L. F. Bosart, 2004: A diagnostic study of jet streaks: Kinematic signatures and relationship to coherent tropopause disturbances. *Mon. Wea. Rev.*, 132, 298–319, https:// doi.org/10.1175/1520-0493(2004)132<0297:ADSOJS>2.0.CO;2.
- Rose, S. F., P. V. Hobbs, J. D. Locatelli, and M. T. Stoelinga, 2004: A 10-yr climatology relating the locations of reported tornadoes to the quadrants of upper-level jet streaks. *Wea. Forecasting*, **19**, 301–309, https://doi.org/10.1175/1520-0434(2004)019<0301: AYCRTL>2.0.CO;2.
- Sanders, F., and D. O. Blanchard, 1993: The origin of a severe thunderstorm in Kansas on 10 May 1985. *Mon. Wea. Rev.*, **121**, 133–149, https://doi.org/10.1175/1520-0493(1993)121<0133: TOOAST>2.0.CO;2.
- Shapiro, M. A., T. Hampel, and A. J. Krueger, 1987: The arctic tropopause fold. *Mon. Wea. Rev.*, **115**, 444–454, https://doi.org/ 10.1175/1520-0493(1987)115<0444:TATF>2.0.CO;2.
- Simmonds, I., and I. Rudeva, 2014: A comparison of tracking methods for extreme cyclones in the Arctic basin. *Tellus*, **66A**, 25252, https://doi.org/10.3402/tellusa.v66.25252.

- Szapiro, N., and S. Cavallo, 2018: Tpvtrack v1.0: A watershed segmentation and overlap correspondence method for tracking tropopause polar vortices. *Geosci. Model Dev.*, 11, 5173– 5187, https://doi.org/10.5194/gmd-11-5173-2018.
- Thompson, D. B., and P. E. Roundy, 2013: The relationship between the Madden–Julian oscillation and U.S. violent tornado outbreaks in the spring. *Mon. Wea. Rev.*, 141, 2087–2095, https://doi.org/10.1175/MWR-D-12-00173.1.
- Tippett, M. K., J. T. Allen, V. A. Gensini, and H. E. Brooks, 2015: Climate and hazardous convective weather. *Curr. Climate Change Rep.*, **1**, 60–73, https://doi.org/10.1007/s40641-015-0006-6.
- Uccellini, L. W., and D. R. Johnson, 1979: The coupling of upper and lower tropospheric jet streaks and implications for the development of severe convective storms. *Mon. Wea. Rev.*, **107**, 682–703, https://doi.org/10.1175/1520-0493(1979)107<0682: TCOUAL>2.0.CO;2.
- —, and P. J. Kocin, 1987: The interaction of jet streak circulations during heavy snow events along the East Coast of the United States. Wea. Forecasting, 2, 289–308, https://doi.org/10.1175/1520-0434(1987)002<0289:TIOJSC>2.0.CO;2.
- Verbout, S. M., H. E. Brooks, L. M. Leslie, and D. M. Schultz, 2006: Evolution of the U.S. tornado database: 1954–2003. Wea. Forecasting, 21, 86–93, https://doi.org/10.1175/WAF910.1.
- Weisman, M. L., and J. B. Klemp, 1982: The dependence of numerically simulated convective storms on vertical wind shear and buoyancy. *Mon. Wea. Rev.*, 110, 504–520, https:// doi.org/10.1175/1520-0493(1982)110<0504:TDONSC> 2.0.CO;2.
- Wernli, H., and M. Sprenger, 2007: Identification and ERA-15 climatology of potential vorticity streamers and cutoffs near the extratropical tropopause. J. Atmos. Sci., 64, 1569–1586, https://doi.org/10.1175/JAS3912.1.
- Wilks, D. S., 2011: Statistical Methods in the Atmospheric Sciences.
 3rd ed. International Geophysics Series, Vol. 100, Academic Press, 704 pp.
- —, 2016: "The stippling shows statistically significant grid points": How research results are routinely overstated and overinterpreted, and what to do about it. *Bull. Amer. Meteor. Soc.*, 97, 2263–2273, https://doi.org/10.1175/BAMS-D-15-00267.1.
- Winters, A. C., and J. E. Martin, 2016: Synoptic and mesoscale processes supporting vertical superposition of the polar and subtropical jets in two contrasting cases. *Quart. J. Roy. Meteor. Soc.*, **142**, 1133–1149, https://doi.org/10.1002/qj.2718.
- —, and —, 2017: Diagnosis of a North American polarsubtropical jet superposition employing piecewise potential vorticity inversion. *Mon. Wea. Rev.*, **145**, 1853–1873, https:// doi.org/10.1175/MWR-D-16-0262.1.